Mapping the indentation between the Iberian and Eurasian plates beneath the Western Pyrenees/Eastern Cantabrian Mountains from receiver function analysis.

J. Díaz[(1)], D. Pedreira[(2)] , M. Ruiz[(1)] , J.A. Pulgar[(2)] and J. Gallart[(1)]

[(1)] Institut de Ciències de la Terra Jaume Almera, ICTJA-CSIC, Barcelona, Spain

[(2)] Departamento de Geología, Universidad de Oviedo, Oviedo, Spain

Abstract

In the last decades, active seismic profiling in the northern part of the Iberian Peninsula have evidenced that the Alpine collision between the Iberian and Eurasian plates resulted in a complex crustal structure, with the Iberian crust underthrusting the Eurasian crust and reaching depths of at least 45-50 km beneath the Pyrenean chain and the Cantabrian Mountains. In the transition between these two zones the situation is particularly complex, as evidenced in previous wide-angle and passive seismic studies. This contribution focuses in getting new clues on the crustal structure of this transitional zone trough receiver functions (RF) analysis of teleseismic data recorded at permanent and temporary stations located in both the Spanish and French sides of the Western Pyrenees. Different techniques (H-κ stacking, pseudo-migration, synthetic 2D modeling) have been considered in the analysis. Passive seismic data from previous temporary deployments in the zone have been reworked and added to the discussion. A first order result is that passive seismic data are broadly consistent with the indentation of the Iberian and Eurasian crusts inferred from active seismic profiling, thus providing a completely independent confirmation of this feature. For the first time, an Iberian Moho underlying the Eurasian crust is documented from RF beneath the stations located

at the Northern side of the Pyrenean range. Moreover, clear indications of dipping interfaces are observed at some stations. The new RF results suggests that in the crustal indentation beneath the Basque Massifs area, the Eurasian crust extends farther south with respect to the image inferred from active seismic data. This new geometry implies that the Pamplona transfer zones has played a major role in the regional geodynamic history.

Introduction

The geodynamic evolution of the Iberian Peninsula has been widely investigated in the last decades and includes Variscan and Alpine compressional events, separated by a large Mesozoic extensional episode. The movement of Iberia relative to Eurasia started already in the Jurassic (eg. Rosenbaum et al., 2002), and resulted in sea floor spreading between chrons M0 and A33o (118-80 Ma) in the western part of the Bay of Biscay. To the east, the rifting stage leads to the development of large sedimentary basins between Iberia and Eurasia, without evidences of oceanization. Transverse structures segmented the through into individual basins along strike. The most prominent of these structures was probably the Pamplona fault, also referred to as the Pamplona transfer zone (PTZ), with present-day orientation NNE-SSW, which marks the eastern limit of the thick Basque-Cantabrian basin (Larrasoaña et al., 2003, Pedreira et al, 2007, Roca et al., 2011) (Figure 1). The convergence between Iberia and Eurasia since late Cretaceous times in the framework of the Alpine orogeny, produced the inversion of those basins and the uplift of basement blocks in the contact zone, building up the Pyrenean-Cantabrian mountain belt, with a limited northward subduction of the Iberian plate (eg. Muñoz, 1992). The transverse transfer structures also played a role during the

compressional stage in partitioning the deformation and the structural style from east to west along the Pyrenean-Cantabrian belt (Pedreira et al., 2007, Roca et al., 2011).

Beneath the central and western Pyrenean chain, active seismic experiments (Gallart et al., 1981, Daignières et al., 1981, 1989, Choukroune et al., 1990, Teixell, 1998) have revealed the crustal features and imbrications between Iberian and Eurasian structures. The Iberian crust deeps northwards and reaches depths of at least 50-55 km, while the Eurasian Moho is observed around 26-30 km depth. The southern limit of this Eurasian crust seems to be located roughly at the vertical of the axial zone of the belt, while the northern limit of the Iberian crust lay a few tens of km northwards. To the West, beneath the Cantabrian Mountains, wide-angle and onshore-offshore seismic data (Pulgar et al., 1996, Fernández-Viejo et al., 1998, Gallastegui et al., 2002, Pedreira et al, 2003) have shown a similar structure, with the imbricated Iberian crust reaching minimum depths of 45-50 km and extending northwards up to the vertical of the coastline. RF analysis of passive seismic data recorded beneath this area has provided images of the crustal structure consistent with these results (Díaz et al., 2009). In the transition between the Pyrenees and the Cantabrian Mountains (longitude range: 1.5W – 4.5W) the structural features are particularly complex, as already evidenced by wide-angle and passive seismic data (Pedreira et al., 2003, Díaz et al, 2003) or gravimetric studies (Pedreira et al., 2007, Jammes et al., 2010). Our purpose in this contribution is twofold; firstly to get new clues on the crustal structure of this area through the RF analysis of teleseismic data provided by the permanent and temporary seismic stations installed in both the Spanish and French sides of the Western Pyrenees-Eastern Cantabrian Mountains in the last decade, and secondly, to provide a state-of-the-art framework for the coming deployments of the Topo-Iberia and PYROPE portable

broad-band seismic networks (http:/iberarray.ictja.csic.es, http://www.dtp.obs-mip.fr/RSSP/PYROPE/).

Data and Methods

Teleseismic data from new permanent stations have been used to calculate receiver functions (RF), and different techniques of processing and analysis (H-κ stacking, pseudo-migration, synthetic 2D modeling) have been considered. We have inspected up to 3 years of available data from 4 broad-band stations of the Spanish IGN network (ELAN, EALK, EARA, EORO) and 4 short period stations belonging to the French Renass-PYRF network (OSSF, ORDF, LARF and ATE). We have also retrieved data from a previous high density, temporary deployment in the zone (Díaz et al., 2003) (Figure 1), because they may help to constrain some features as shown in the discussion, despite the limited duration of these experiments and the scarce amount of available data.

The first step was selecting teleseismic events with magnitude higher than 5.5, epicentral distances between 35º and 95º and clear P arrivals. We then calculated the corresponding RF by frequency domain deconvolution (Langton, 1979) of the vertical component from the horizontal components in the time window corresponding to the P arrival and its coda. The deconvolution was performed using the classical "pwaveqn" software (Ammon, 1997), using gauss filter-width parameter values of 2-4 and typical water level values ranging between .01 and .001. The parameters used for the gauss filter represent pulse widths of 1.2-0.83 s at half-maximum amplitude. After visual inspection, only those RF with good signal-to-noise ratio were retained (Table 1). For

the permanent stations the number of RFs analyzed ranges between 23 and 77, while for the temporary array only 12 RFs on average are retained for each station.

We have used the H-κ analysis (Zhu and Kanamori, 2000) to infer an estimation of the crustal depth (H) and the κ ratio ($\kappa = v_p/v_s$) beneath each investigated station. This method, nowadays widely used, considers a mean crustal velocity and estimates the arrival time of the Ps, PpPs and PsPs phases for each given combination of H and κ. The amplitude of the real RFs at those times is then evaluated in the (H, κ) parameter space. The presence of a well-defined maximum in the stacking surface defines the preferred solution for each station. In many cases, and especially if the energy of the multiple phases is scarce, the trade-off between both parameters produces stacking surfaces showing a well defined "crest" but with poorly constrained maximum value. We have used a mean crustal v_p=6.3 km/s, estimated from the wide-angle seismic profiles available in the region (Gallart et al., 1981, Pedreira et al., 2003). It has been shown that variations of +/- 0.1 km/s in v_p result in changes of +/- 0.6 km in the Moho depth, making the choice of the reference v_p value not a critical issue (Mohsen et al., 2005; Nair et al., 2006).

The retrieval of RF values is restricted in principle to zones with sub-horizontal, isotropical crustal structure, as it is based on the assumption that the vertical component deconvolution removes the signature of the source time function and the possible source-side and deep-earth propagation effects. Under this hypothesis, no signal is expected in the transverse RF components. However, it has been widely proved that RF can also be useful to investigate the crustal structure in zones with dipping layers and/or anisotropy. In this case, the transverse RFs have clear arrivals and both the radial and

transverse RFs show azimuthal variation patterns in their polarity and amplitude that can be used to discern between dipping boundary and anisotropic origin (e.g. Savage, 1998).

Previous active and passive seismic results suggest that beneath the Pyrenean-Cantabrian ranges the Iberian and Eurasian crusts are imbricated and, consequently, two Mohos could be identified as major discontinuities (Pedreira et al., 2007, Díaz and Gallart, 2009). In order to check the corresponding image expected from the H-κ technique in such a case of a "double Moho", we considered a synthetic approach in which RF are constructed using the Raysum package (Frederiksen and Bostock, 1999) from a 1D velocity-depth model with a typical κ value of 1.73, a 20 km thick upper crust (v_p=6.2 km/s), a 10 km thick lower crust (v_p=6.6 km/s), a 7 km thick European mantle wedge (v_p=7.8 km/s), a low velocity zone with v_p=6.8 km/s representing the Iberian lower crust and a 6.8 to 8.1 km/s discontinuity at 44 km depth (Figure 2a). The H-κ method is then applied to those synthetic RFs. The result (Figure 2b) shows two clear local maxima in the stacking surface. The deeper Moho provides the best constrained one, but its position is underestimated (41.5 vs. 44 km) and the κ value is overestimated (1.76 vs. 1.73). This is probably related to the multiples generated at the upper discontinuities that interfere with the conversions at this level. The upper Moho is identified by a less well-defined correlation maximum in the H-κ diagram, resulting in a "crest" with a local maximum located at h=30.5 km and a κ value of only 1.68. Even if the resolution is poor for this upper convertor, the method provides a good estimation of its depth. The presence of two maxima in stacking surfaces derived from real data can therefore be interpreted as evidence of two relevant discontinuities with strong velocity contrasts across them, which may correspond to a "double-Moho" structure. Note that

the synthetic RF (Figure 2c) shows a negative peak at about 4.2 s, between the arrivals of the two Mohos, arising from the low velocity zone introduced between them to represent the Iberian lower crust underlying the Eurasian mantle wedge.

In order to get structural information comparable to the seismic reflection sections, the obtained RFs can be treated using a Common Conversion Point procedure to obtain images of the lithosphere in depth domain. The RFs from a single station or from neighboring stations are traced back along their raypaths using a 1D velocity model, the amplitudes contributing to each cell of the model are stacked and the data is projected along a profile. The amplitude contrast in the final images depicts the zones where incoming waves suffer P to S conversions (see Figure 3). Those images are useful to identify lateral variations in the spatial location of the main convertors.

Results

Beneath the Cantabrian Mountains, station ELAN shows evidences of dipping in the Moho interface, including energy in the transverse RF and amplitude changes in the Ps arrivals both in the radial and transverse RFs. To better analyze these features, RFs have been corrected for Ps moveout with a reference slowness of 6.4 s/deg and then stacked into bins of 10º of backazimuth, with an overlap of 5º (Figure 3a). The amplitude of the Ps arrival on the radial component changes with the backazimuth. Synthetic tests have shown that models with a Moho dipping 10º northward can explain these amplitude variations, even if the limited azimuthal coverage makes it difficult to evaluate precisely the dipping direction, which may vary from NW to NE. The amplitudes in the transverse component are much weaker, but polarization changes in the P arrival can still be observed, while the Ps arrivals are difficult to identify (Figure 3b). The negative

pulses observed at t=0 for backazimuths between N30ºW and N70ºE would require, in our simple dipping model, a dip direction oriented N60ºE to N90ºE. This is neither compatible with the observations in the radial RF nor with the polarization changes of the transverse Ps phase. However, it must be taken into consideration that the amplitude of the transverse component in the synthetic models is about 5 times smaller than the amplitude of the radial RF and thus, the real signal can be easily contaminated by noise. Even if the results are not conclusive, a Moho dipping 10º northward can account for most of the observations. The H-κ analysis (Figure 3c) displays two prominent maximum correlation crests, corresponding to major discontinuities that we interpret as the signature of the Iberian and Eurasian Mohos, which would be located at 28 and 49 km depth respectively. In this interpretation, the presence of Iberian lower crustal materials underthrusting the mantle will act as a low velocity zone, resulting in a large negative conversion in the RFs before the main Ps arrival. This feature can be observed in the RFs reaching ELAN from N20ºW to N30ºE backazimuths, but not in those coming from South to West azimuths (Figure 3a), arguing in favour of a northward dipping of the Iberian Moho. This azimuthal difference is consistently observed in the image retrieved from the N-S projected pseudo-migrated section (Figure 3d). The Eurasian Moho corresponds to the horizontal converter at 30 km depth in the northern part of the section, while the Iberian Moho can be associated with the main deep converter, which seems to dip from 45 km in the South to 50 km at the northern termination of the section. The convertors close to 15 km depth in the northern section and at 25 and 35 km depth in the southern part can be associated to intracrustal seismic discontinuities previously imaged by active seismic profiles (Pedreira et al., 2003). A North-South oriented 2D velocity-depth model derived from the MARCONI deep seismic sounding experiment in the Bay of Biscay (Ruiz et al., 2007), shows an

European Moho at around 28 km depth that can be followed southwards until 10 km to the north of ELAN station, whereas the position of the Iberian Moho along this profile is not well constrained. On the other hand, in an E-W refraction profile that runs about 17 km to the south of ELAN (Pedreira et al., 2003), the Iberian Moho is located at ~39 km depth and the top of the lower crust at ~27 km. The 3D gravimetric model constructed with these and other seismic constraints locates the Moho at 44.5 km beneath ELAN, dipping northwards down to 54 km (Pedreira et al., 2007). According to this model, the top of the Iberian lower crust is found at ~32 km beneath ELAN, a feature that may be related to the third (and less pronounced) local maximum in the H-κ diagram, located at H=38 km. Hence, the values here inferred have an overall consistency with available seismic and gravimetric models, even if the convertors appear to be some kilometers deeper. The absence of clear PmP constraints on this particular part of the Iberian side and the lack of resolution of the RF methods in an area of crustal complexity may account for that discrepancy.

For the stations located at the northern side of the Pyrenean chain (OSSF, ORDF, LARF, ATE) the H-κ analysis reveals quite coherent results, with a first order convertor located at 46-53 km, interpreted as the Iberian Moho, which results in a large amplitude Ps arrival at 5.7 to 6.5 s after the P phase (Figures 4a, 4b). A secondary maximum with a much weaker signature can be identified in the stacking surface, corresponding to an interface located at 26-28 km for the stations in the North Pyrenean Zone (OSSF, ORDF) and 27-29 km for stations in the Axial zone (LARF, ATE), (Figure 4a, 4b, Table 2). These values are close to the Moho depths of 25-27 km reported by Daignières et al. (1981) in an East-West refraction profile along the North Pyrenean Zone. Hence, in the study area the Iberian Moho extending beneath stations

on the North Pyrenean Zone is identified for the first time from an RF analysis, whereas the stations beneath the Axial Zone are depicting the southern extent of the Eurasian Moho indentation. The negative amplitude peak associated to the discontinuity between the mantle wedge and the Iberian lower crust is observed in some cases, as for example in station ATE (see stacked trace in Figure 4b), while in other cases it may be masked by the complexity of the RFs.

Stations at the Southern side of the Pyrenees (NAP, EARA, EUG, EORO) display a simpler image, with a well-defined, single maximum peak for H values of 39-44 km (Figure 4c, Table 2). These crustal depths are broadly compatible with the results from active seismic profiles in the zone (Gallart et al., 1981, Pedreira et al., 2003) and are clearly shallower than those inferred at the stations located in the Northern side, revealing a North-dipping Iberian Moho.

To the west of the Pamplona Fault, in the Basque-Cantabrian region, H-κ analysis at temporary station BER displays a well-defined Moho at around 32 km depth (Figure 4d). This is consistent with results from available data of neighboring ARA and IBA stations of the same experiment. This relatively thin crust may be interpreted as a portion of the Eurasian crust indenting Iberia farther south than in the previously discussed area, eastwards. The H-κ analysis shows a weak secondary maximum at 52 km depth beneath BER, which can be interpreted consistently with active seismic methods as depicting the Iberian Moho. Data from the permanent station EALK, located about 20 km east of those stations, evidence again a complex crustal structure. Azimuthal variations can be observed in both the radial and transverse components, probably reflecting the presence of dipping convertors and heterogeneities (Figure 5a).

Similarly as for station ELAN, a clear negative peak in the radial RFs can be observed only for events with N20ºW to N110ºE backazimuths. This argues in favor of the hypothesis of an Iberian lower crust underthrusting the mantle northwards. Nevertheless, H-κ analysis of the complete data set provides a well-defined convertor, located at 43 km depth (Figure 5c). A pseudo-migrated depth section of these data along an E-W profile (Figure 5b) illustrates this clear convertor and suggest a shift of about 5 km between events coming from eastern and western backazimuths, even if more data should be necessary to confirm this point. The interpretation of this convertor is not clear, as seems too shallow to be related to the Iberian Moho. The velocity-depth model obtained from the late 70s wide-angle profile along the Pyrenean Basque Massifs (Gallart et al., 1981), evidenced the European Moho located at 30 km near the coast and the Iberian Moho at about 50 km depth further East, with the border between both areas located close to the position of EALK. The anomalous depth of the main convertor beneath EALK and the complex azimuthal variations observed may result from the presence, very close to the station, of a significant discontinuity at Moho depths in E-W direction. In spite of these complexities, it can be concluded that the zone covered by stations BER, IBA, ARA and limited by station EALK depicts an area of a pronounced southward indentation of the Eurasian crust, the eastern limit of which is represented by the Pamplona transfer zone (PTZ). Figure 6 presents three pseudo-migrated profiles oriented parallel to the PTZ, two of them located East of this accident and the last one immediately West of it. The eastern sections show a dipping Iberian Moho reaching depths exceeding 50 km beneath the Pyrenean chain, with a weak signal from the European Moho at about 30 km in northern end of the sections. The continuity of the Iberian Moho is clearer and more consistent with wide-angle profiling results (Gallart et al., 1981; Pedreira et al., 2003) in the easternmost section, as the middle one include the

EALK station, whose complex results have been discussed previously. The profile located west of the PTZ shows a more complex pattern. The most prominent feature in this case is a well-imaged convertor located at about 30 km depth in the northern side, which can be easily interpreted as the European Moho. It can be followed to the south as far as beneath station BER, where it seems to connect a broad (10-15 km thick) positive and north-dipping anomaly, the interpretation of which is doubtful due to the lack of resolution and strong complexities in the velocity structure revealed by previous wide-angle data west of the PTZ, where even the Iberian Moho is not a clear feature (Pedreira et al., 2003).

The Poisson's ratio (σ), directly derived from the Vp/Vs ratio, is often used to estimate the composition of the crust, as it is more sensitive to mineralogical changes than single P or S wave velocities (p.e. Christensen, 1996). Crustal composition is generally divided into categories of low Poisson's ratios ($\sigma < 0.26$), intermediate values ($0.26 < \sigma < 0.28$), and high values ($\sigma > 0.28$) (Holbrook et al., 1992). Low Poisson's ratios suggest a more felsic composition, whereas high values generally correspond to a more mafic crust. Our σ results, presented in Table 2, show that the crust in the investigated area has in general a low Poisson's ratio, with a mean value of 0.252. This is consistent with the mean value of 0.25 +/- 0.04 reported by Zandt and Ammon (1995) for Mesozoic-Cenozoic regions of active or recent tectonics. The large error bars associated to the Vp/Vs determination do not allow entering in further discussion on differences between the different stations. However, it is interesting to note that the higher value of σ (0.273) is obtained at stations ORDF, LARF and ATE, close to the area where Daignières et al. (1981) reported a very high Poisson's ratio for the upper crust, reaching values of 0.32-0.33 (Vp/Vs=1.9-2.0) that was tentatively associated to

sediments with high water content. The presence in this area of several outcrops of ultramafic rocks exhumed from the upper mantle during the cretaceous rifting stage between Iberia and Eurasia (eg. Jammes et al., 2009) and a positive gravimetric anomaly interpreted to be caused by uplifted lower crustal/mantle material (Grandjean, 1994; Casas et al., 1997; Pedreira et al., 2007; Jammes et al., 2010), seem to indicate the occurrence of large mafic/ultramafic bodies within the upper crust that can also be at least a partial explanation for these high Poisson's ratios.

Discussion and Conclusions

A first order result of this contribution is that passive seismic data are broadly consistent with structural features of the Iberian and Eurasian crusts inferred from active seismic profiling (Figure 7a) and thus provides a completely independent confirmation of the indentation between both crusts. In regions of simple crustal structure, RF and H-κ modeling constitute very powerful and affordable methods to highlight the main crustal features, but even in complex areas like the one studied in this paper, they have been proved to be very efficient when combined with other seismic constraints, and may help to extend the two-dimensional interpretations of active seismic profiling to the three dimensions. In the western Pyrenees, the analysis of the data recorded at the northern side of the range has allowed to document, for the first time from RF analysis, the presence of the Iberian Moho at depths around 50 km, underlying the Eurasian Moho, which appears as a secondary convertor located at 25-35 km depth. Beneath the central Pyrenees and the Cantabrian Mountains, previous active and passive seismic results provide a similar image of the crustal structure, including clear evidences of northward oriented dipping of the Iberian Moho (Díaz et al., 2003, 2009, Pedreira et al., 2003).

Beneath the Pyrenean Basque Massifs, in the area delimited by the Pamplona and Hendaya faults (the later being subparallel to the Pamplona fault and located about 50 km westward), the geometry of the indentation of both crusts previously reported should be modified according to the present RF results. Temporary stations at the Basque Massifs show a shallow Moho (31-32 km) that is interpreted as an evidence of the Eurasian crust indenting the Iberian crust farther south than the geometry delineated by Pedreira et al. (2007), and at least as south as the location of station BER (piercing points of ray paths crossing the Eurasian Moho are located at latitudes close to or north of this point). The Iberian Moho is difficult to identify in this very complex area, the eastern limit of which was sampled by station EALK, but become the most prominent feature to the east of it, where the European Moho has a much weaker signature. This significant change in the crustal structure is geographically coincident with the PTZ. This feature, without a clear surface expression, has probably a Late-Variscan origin and played a major role already in Mesozoic times, actively controlling the deposition of several kilometers of sediments more in the western block (the Basque-Cantabrian Basin) than in the eastern one (eg. Larrasoaña et al., 2003). The depocenter in the core of the Basque-Cantabrian Basin is shifted southwards with respect to the main one in the Labourd-Mauléon area, at the other side of the PTZ (Jammes et al., 2009). The partition of the deformation during the Cenozoic Alpine compressional event is evident, since structures with northward vergence predominate in the western block whereas those with southward vergence are dominant in the eastern side. The PTZ is also evidenced by other geological and geophysical data sets. Detailed seismicity maps (Figure 7b) show that the Pamplona transfer zone corresponds to a clear western limit of the seismic activity beneath the Pyrenean chain. East of 1ºW, the seismicity is concentrated along the North-Pyrenean Zone and the northern border of the axial zone.

Further west (1ºW to 2ºW), it is sparser, with significant events in the southern side of the chain and along the trace of the Pamplona fault. West of the Hendaya fault, the seismicity decreases abruptly with only few sparse events. Detailed regional seismic studies using temporal networks have confirmed these features (Ruiz et al., 2006a, 2006b). The propagation of crustal phases across this zone of the western Pyrenees shows an anomalously strong attenuation, whose origin has been related to a crustal region with increased heterogeneity and intrinsic attenuation due to a strong deformation process (Sens-Schönfelder et al., 2009). The gravimetric anomaly map (Pedreira et al., 2007) shows two zones of positive anomaly values clearly related to the Basque-Cantabrian and the Mauleon basins. The area here investigated appears as a slightly negative gravimetric anomaly located between those basins and delimited by the Pamplona and Hendaya transfer zones. Finally, the magnetic map (Pedreira et al., 2007) shows a clear positive anomaly North of Vitoria. This magnetic feature, one of the most prominent in the whole Iberian Peninsula, seems also to be bounded by the Hendaya fault. The new passive seismic data seem to confirm that the Pamplona and Hendaya transfer zones have played a major role in the regional geodynamic history, and allow delineating in a more precise way the changes in crustal thickness and internal structure across these transverse structures, which seem to be more abrupt and relevant than previously thought. The deployment of the Topo-Iberia and the PYROPE seismic networks will hopefully provide additional constraints on the structure of this very complex collision zone between the Iberian and Eurasian plates.

Acknowledgments

Most of the figures were created using GMT software (Wessel and Smith, 1998). This is a contribution of the Consolider-Ingenio 2010 project TOPO-IBERIA (CSD2006-00041).

Figure captions

Figure 1: Simplified geological map showing the location of the seismic stations and the main geological units. BCB: Basque-Cantabrian Basin. HF: Hendaya Fault. PTZ: Pamplona transfer zone. Cv, Lab, Ald: Cinco Villas, Labourd and Aldudes Basque Massifs. MB: Mauléon Basin. NPZ: North Pyrenean zone. SPZ: South Pyrenean Zone. The North and South Pyrenean frontal thrusts are also depicted.

Figure 2: a) Velocity-depth model used for the synthetic modeling. b) H-κ analysis of the resulting RF. The color scale refers to the percentage of the maximum staked amplitude. The two maxima can be related to the two first order positive discontinuities in the model. c) Radial receiver function obtained from this model. The positive peaks at 3.3 and 5.1 s correspond to the two Mohos, while the negative peak in-between is generated by the low velocity zone.

Figure 3: Results for station ELAN. a,b) RFs retrieved from the radial and transverse components, corrected for Ps moveout and stacked into bins of 10º of backazimuth with an overlap of 5º. The bottom part of each panel shows the radial and transverse stacked RFs. c) H-κ analysis. d) pseudo-migrated section.

Figure 4: H-κ analysis for stations located in the North Pyrenean zone (a,b), the South Pyrenean zone (c) and the transitional zone (d). Black ellipses denote the estimated error. The bottom part of each panel shows the stacked radial RF for that station.

Figure 5: Station EALK. a) Radial and transverse RFs sorted by backazimuth. b) Pseudo-migrated depth section c) H-κ analysis.

Figure 6: Three pseudo-migrated sections oriented subparallel to the Pamplona Tranfer Zone. The differences in the geometry of the convertors from east to west are clearly observed.

Figure 7: a) Moho depths as derived from our H-κ analysis (white circles) compared with those derived from wide-angle profiling (light blue circles). Solid and dashed red lines depict respectively the presently inferred and the previously proposed southward limit of the Eurasian crust after Pedreira et al. (2003, 2007). Blue line shows the northward limit of the Iberian crust. The main geological units, including the position of the Pamplona and Hendaya transfer zones, are represented as in Figure 1. b) Regional seismicity map. Blue dots: RENASS catalog (1989-2004) Red dots: IGN catalog (1989-2004).

References

Ammon, C.J. (1997). An overview of receiver function analysis. http://eqseis.geosc.psu.edu/~cammon/HTML/RftnDocs/rftn01.html

Choukroune, P., F. Roure, B. Pinet and ECORS Pyrenees Team, (1990). Main results of the ECORS Pyrenees profile. Tectonophysics, 173, 1-4, 20, 411-418.

Christensen, N. I. (1996), Poisson's ratio and crustal seismology, J. Geophys. Res., 101, 3139–3156, doi:10.1029/95JB03446.

Daignières, M., Gallart, J. and Banda, E. (1981). Lateral variation of the crust in the North Pyrenean Zone. Annales Geophysique, 37, 3, 435-456.

Daignières, M., de Cabissole, B., Gallart, J., Hirn, A., Surinach, E. and Torné, M., (1989). Geophysical constraints on the deep structure along the ECORS Pyerenees line. Tectonics, 8, 5, 1051-1058.

Díaz, J. Gallart, J., Pedreira, D., Pulgar, J.A., Ruiz, M., López, C. and González-Cortina, J.M. (2003) Teleseismic imaging of alpine crustal underthrusting beneath N-Iberia. Geophys. Res. Let., 30, 11, doi: 10.1029/2003GL017073

Díaz, J., J. Gallart, J.A. Pulgar, M. Ruiz and D. Pedreira (2009). Crustal structure beneath North-West Iberia imaged using receiver functions. Tectonophysics, 478, 3-4, 175-183, doi:10.1016/j.tecto.2009.08.003

Díaz, J. and Gallart, J. (2009). Crustal structure beneath the Iberian Peninsula and surrounding waters: a new compilation of deep seismic sounding results. Phys. Earth Planet. Int., 173, 181-190 doi:10.1016/j.pepi.2008.11.008

Fernández-Viejo, G., J. Gallart, J. A. Pulgar, J. Gallastegui, J. J. Dañobeitia, and D. Córdoba (1998), Crustal transition between continental and oceanic domains along the North Iberian Margin from wide angle seismic and gravity data, Geophys. Res. Lett., 25(23), 4249–4252, doi:10.1029/1998GL900149.

Frederiksen, A.W. and Bostock, M.G. (1999). Modelling teleseismic waves in dipping anisotropic structures, Geophys. J. Int., 141, 401–412.

Gallart, J., E. Banda, and M. Daignères (1981), Crustal structure of the Paleozoic Axial Zone of the Pyrenees and transition to the North Pyrenean Zone, Ann. Geophys., 37(3), 457– 480.

Gallastegui, J. (2000), Estructura cortical de la Cordillera y Margen Continental Cantabricos: Perfiles ESCI-N, Trabajos Geol., 22, 9– 234.

Gallastegui, J. Pulgar, J. and Gallart, J., (2002). Initiation of an active margin at North Iberian continent-ocean transition. Tectonics, 21(4), 1033, doi:10.1029/2001TC901046

Holbrook, W. S., W. D. Mooney, and N. I. Christensen (1992), The seismic velocity structure of the deep continental crust, in Continental Lower Crust, edited by D. M. Fountain, R. Arculus, and R. Kay, pp. 1–43, Elsevier Science Publishers, Amsterdam.

Jammes, S., Manatschal, G., Lavier, L. and Masini, E. (2009), Tectonosedimentary evolution related to extreme crustal thinning ahead of a propagating ocean: Example of the western Pyrenees. Tectonics, 28, TC4012, doi:10.1029/2008TC002406.

Jammes, S., Tiberi, Ch and Manatschal, G., (2010). 3D architecture of a complex transcurrent rift system: The example of the Bay of Biscay–Western Pyrenees. Tectonophysics, 489, 210–226

Langston,C.A. (1979). Structure under Mount Rainier, Washigton, inferred from teleseismic body waves. J. Geophys. Res., 84, 4749-4762.

Larrasoaña, J.C., Parés, J.M., del Valle, J., Millán, H., (2003). Triassic paleomagnetism from the western Pyrenees revisited; implications for the Iberian-Eurasia Mesozoic plate boundary. Tectonophysics 362, 161–182

Mohsen, A., Hofstetter, R., Bock, G., Kind, R., Weber, M., Wylegalla, K., and Rümpker, G. (2005). A receiver function study across the Dead Sea Transform. Geophys. J. Int., 160(3), 948-960. doi:10.1111/j.1365-246X.2005.02534.x

Muñoz, J. A. (1992), Evolution of a continental collision belt: ECORS Pyrenees crustal balanced cross-section, in Thrust Tectonics, edited by K. R. McClay, pp. 235– 246, Chapman and Hall, Boston, Mass.

Nair, S. K., Gao, S. S., Liu, K. H., and Silver, P. G. (2006). Southern African crustal evolution and composition: Constraints from receiver function studies. Journal of Geophysical Research, 111(B2), 1-17. doi:10.1029/2005JB003802

Pedreira, D., Pulgar, J.A., Gallart, J. and Díaz, J., (2003). Seismic evidence of Alpine crustal thickening and wedging from the western Pyrenees to the Cantabrian Mountains (north Iberia). Journal of Geophysical Research, 108 (B4), 2204, doi:10.1029/2001JB001667.

Pedreira, D., Pulgar, J.A., Gallart, J., Torné, M., 2007. Three-dimensional gravity and magnetic modeling of crustal indentation and wedging in the western Pyrenees–Cantabrian Mountains. J. Geophys. Res. 112, B12405. doi:10.1029/2007JB005021.

Pulgar, J.A., Gallart, J., Fernández-Viejo, G., Pérez-Estaún, A., Álvarez-Marrón, J. and ESCIN Group, (1996). Seismic image of the Cantabrian Mountains in the western extension of the Pyrenean belt from integrated reflection and refraction data. Tectonophysics, 264,1-19.

Roca, E., Muñoz, J.A., Ferrer, O and Ellouz, N. (2011). Tectonics, 30, TC2001, doi:10.1029/2010TC002735.

Ruiz, M., (2007). Caracterització estructural i sismotectònica de la litosfera en el domini Pirenaico-Cantàbric a partir de métodes de sísmica activa i pasiva, Ph. Thesis, Univ. Barcelona. 353 pp.

Ruiz, M , Gallart, J., Díaz, J., Olivera, C., Pedreira, D., López, C., González-Cortina, J.M. and Pulgar, J.A. (2006a). Seismic activity in the Western Pyrenean edge. Tectonophysics, 412, 3-4, 217-235, doi:10.1016/j.tecto.2005.10.034.

Ruiz, M., Gaspà, O., Gallart, J., Díaz, J., Gallart, J., Pulgar, J.A., García Sansegundo, López-Fernández, C. and González-Cortina, J.M. (2006b). Aftershocks Series Monitoring of the September 18, 2004 4.6 Lg Earthquake at the Western Pyrenees: a case of Reservoir-Triggered Seismicity. Tectonophysics, 424, 223-243, doi:10.1016/j.tecto.2006.03.037

Savage, M.K, 1998. Lower crustal anisotropy or dipping boundaries? Effects on receiver functions and a case study in New Zealand. J. Geophys. Res., 103, 15069-15087.

Sens-Schönfelder, C., Margerin, L., and Campillo, M. (2009). Laterally heterogeneous scattering explains Lg blockage in the Pyrenees. Journal of Geophysical Research, 114(B7). doi:10.1029/2008JB006107

Teixell, A. (1998). Crustal structure and orogenic material budget in the west central Pyrenees. Tectonics 17 (3), 395–406.

Wessel, P., and W. H. F. Smith (1998), New, improved version of the generic mapping tool released, EOS Trans., AGU, 79, 579.

Zandt, G and Ammon, C.J. (1995). Continental crust composition constrained by measurements of crustal Poisson's ratio. Nature, 374, 152-154.

Zhu, L. and H. Kanamori (2000). Moho depth variation in southern California from teleseismic receiver functions, J. Geophys. Res. 105, 2969–2980.

Table 1

Station	*Network*	*Sensor*	*Time period analysed*	*No of retained RFs*
ELAN	IGN	CMG3T (120s)	2007-2009	77
EARA	IGN	CMG3T (120s)	2007-2009	77
EALK	IGN	CMG3T (120s)	2007-2009	31
EORO	IGN	CMG3T (120s)	2008-2009	34
ORDF	PYRF (Renass)	L4-3D (1 Hz)	2007-2009	23
OSSF	PYRF (Renass)	L4-3D (1 Hz)	2007-2009	49
LARF	PYRF (Renass)	L4-3D (1 Hz)	2007-2009	74
ATE	PYRF (Renass)	L4-3D (1 Hz)	2007-2009	36
IBA	Temporary	Le5s (5s)	3-8/1999	6
ZUG	Temporary	Le5s (5s)	9/2000-6/2001	11
ARA	Temporary	Le5s (5s)	3-8/1999 9/2000-6/2001	11
BER	Temporary	Le5s (5s)	3-8/1999 9/2000-6/2001	16
EUG	Temporary	Le5s (5s)	3-8/1999	9
NAP	Temporary	Le5s (5s)	6-7/1999 9/2000-6/2001	18

Table 2

Station	***Moho depth***	κ	Poisson ratio
ELAN *	28 +/- 2 49 +/- 2.5	1.75 +/- 0.05 1.70 +/- 0.07	0.258 0.235
EARA	40 +/- 3	1.75 +/- 0.09	0.257
EALK	43 +/- 2	1.73 +/- 0.04	0.249
EORO	44 +/- 3	1.75 +/- 0.07	0.258
ORDF *	28 +/- 2 47 +/- 2	1.79 +/- 0.08 1.78 +/- 0.07	0.273 0.269
OSSF *	26 +/- 2 53 +/- 3	1.73 +/- 0.06 1.73 +/- 0.04	0.253 0.249
LARF *	29 +/- 2 48 +/- 3	1.78 +/- 0.07 1.72 +/- 0.06	0.269 0.245
ATE *	27 +/- 1.5 46 +/- 1.5	1.79 +/- 0.06 1.77 +/- 0.05	0.273 0.266
IBA	31 +/- 3	1.71 +/- 0.07	0.240
ZUG	28 +/- 2	1.74 +/- 0.06	0.253
ARA	32 +/- 2	1.74 +/- 0.06	0.245
BER	32 +/- 2	1.75 +/- 0.06	0.258
EUG	39 +/- 3	1.75 +/- 0.07	0.258
NAP	44 +/- 2	1.70 +/- 0.04	0.235

* Stations with two main convertors, interpreted as corresponding to the Eurasian and Iberian Mohos

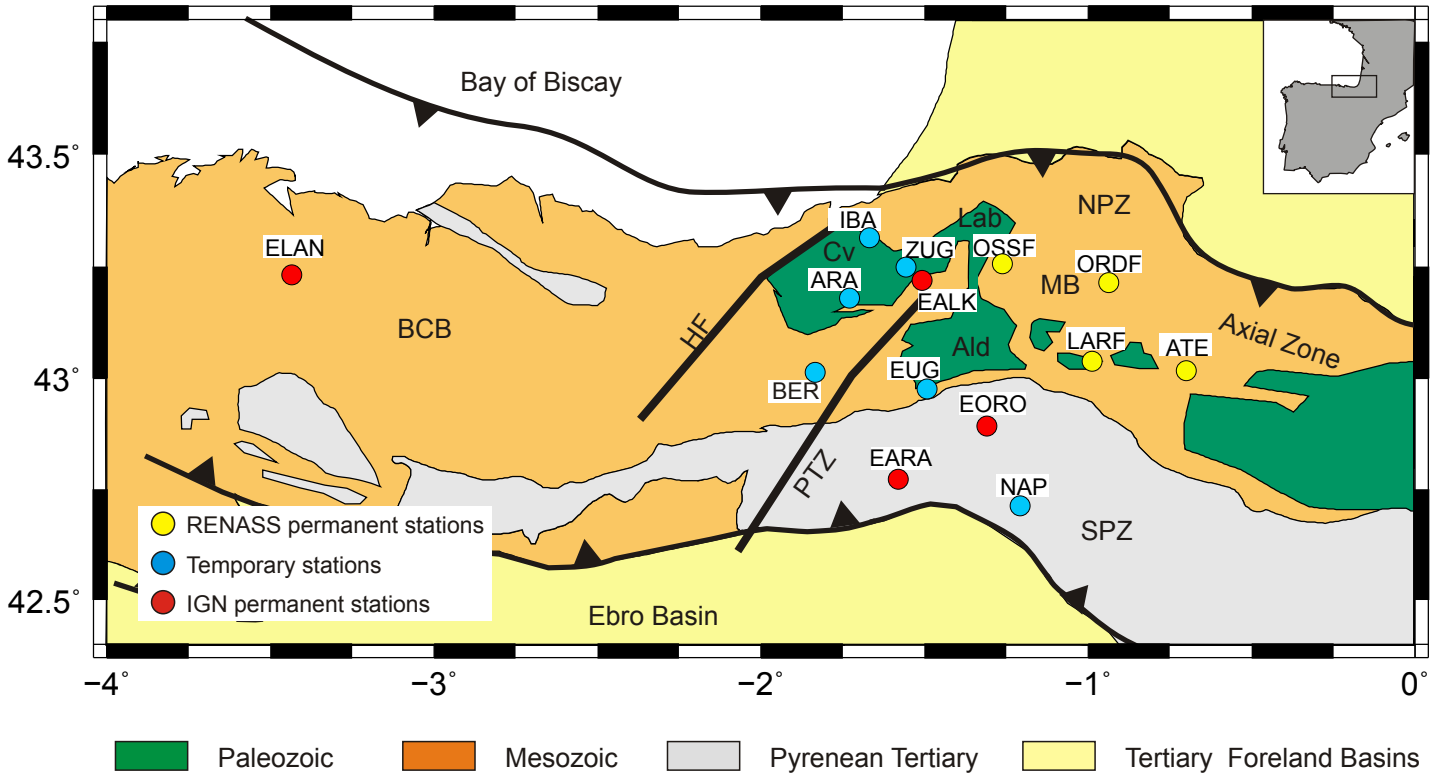
Bay of Biscay
43.5˚
43˚
42.5˚
−4˚
−3˚
−2˚
−1˚
0˚
ELAN
BCB
IBA
Cv
ZUG
ARA
EALK
Lab
OSSF
NPZ
ORDF
MB
HF
Ald
LARF
ATE
Axial Zone
EUG
BER
EORO
EARA
PTZ
NAP
SPZ
Ebro Basin
RENASS permanent stations
Temporary stations
IGN permanent stations
Paleozoic
Mesozoic
Pyrenean Tertiary
Tertiary Foreland Basins

Figure 1

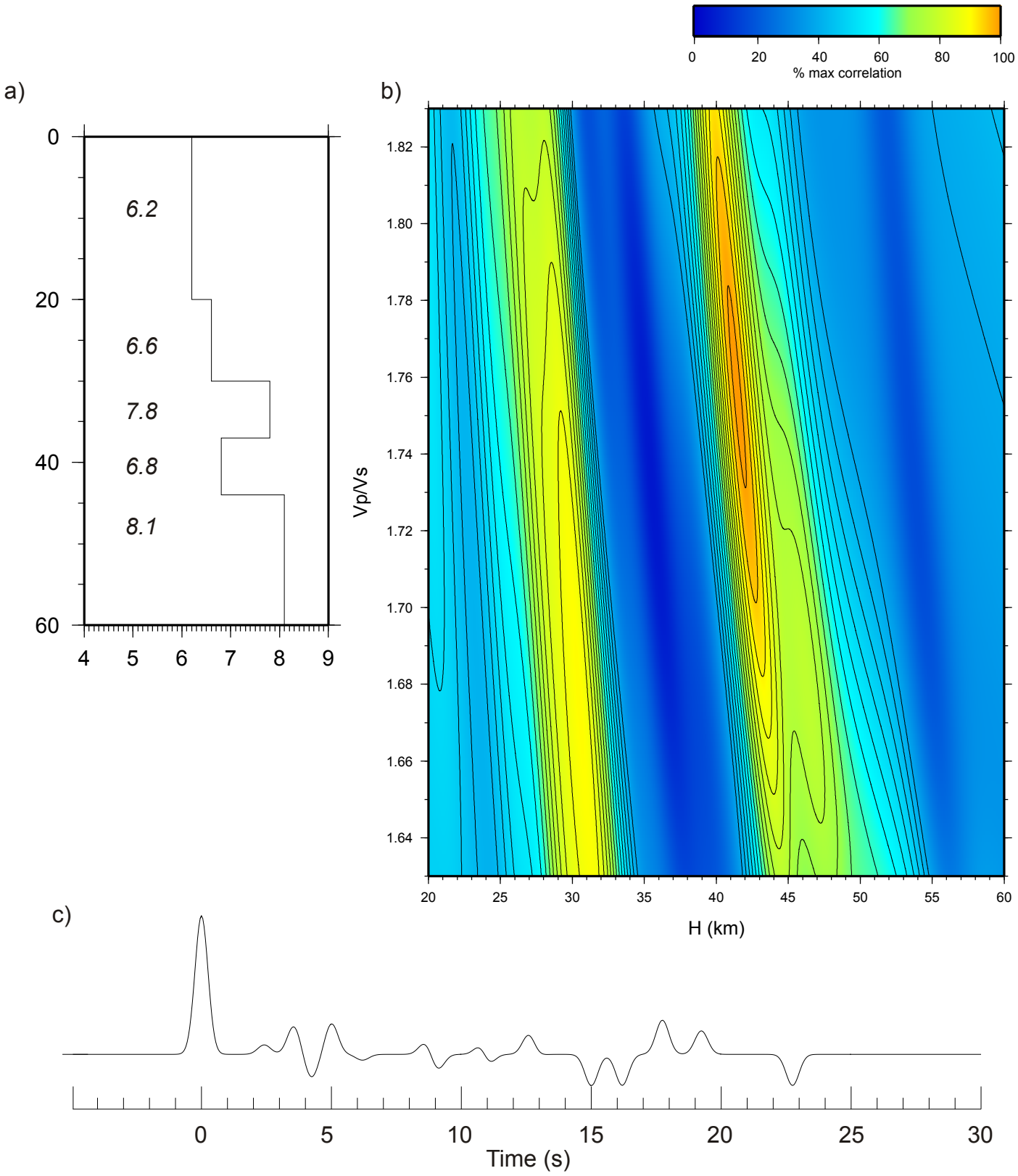
a)
b)
c)
0
20
40
60
6.2
6.6
7.8
6.8
8.1
4
5
6
7
8
9
% max correlation
0
20
40
60
80
100
Vp/Vs
1.82
1.80
1.78
1.76
1.74
1.72
1.70
1.68
1.66
1.64
20
25
30
35
40
45
50
55
60
H (km)
0
5
10
15
20
25
30
Time (s)

Figure 2

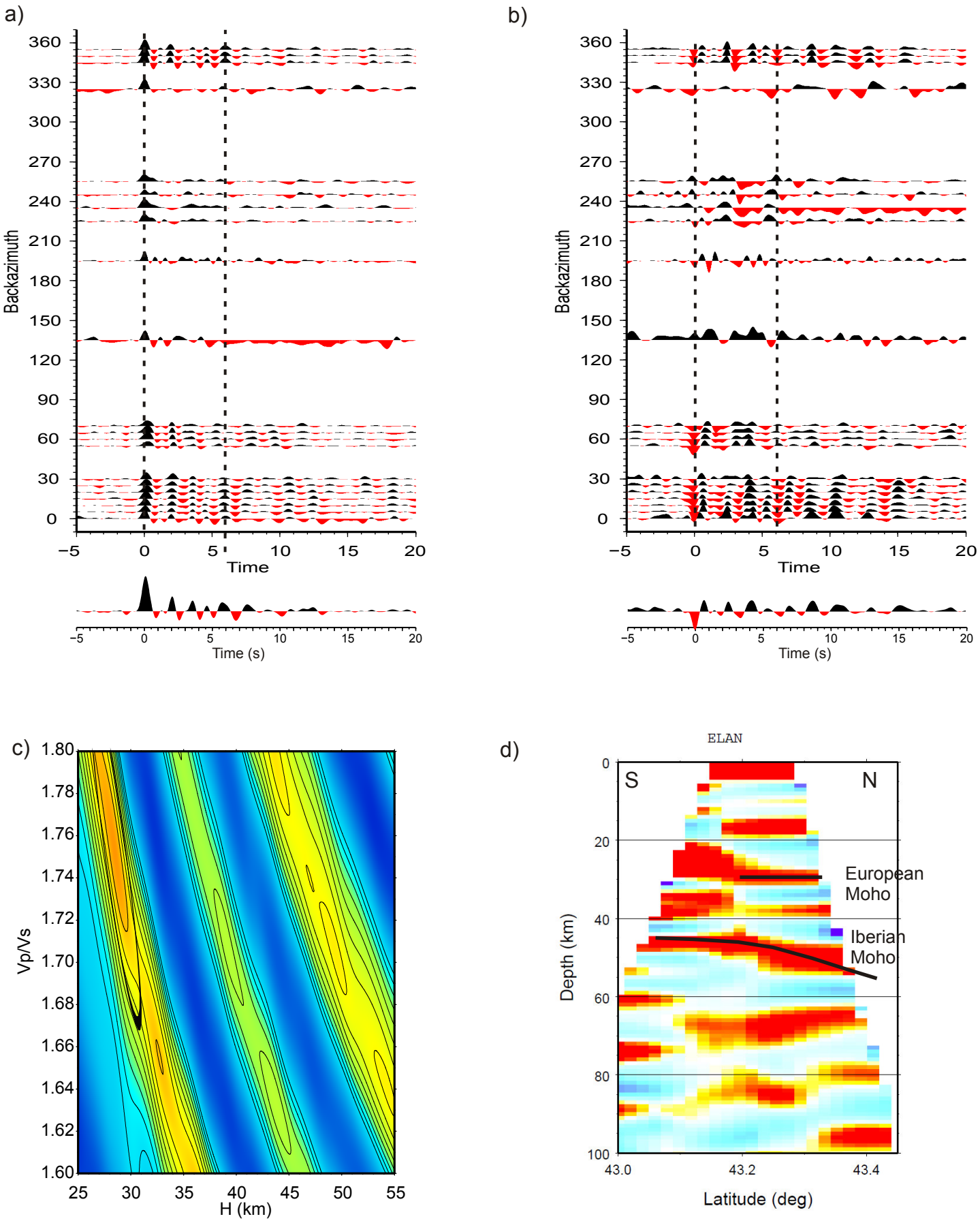
a)
b)
Backazimuth
Time
Time (s)
c)
Vp/Vs
H (km)
d)
ELAN
S
N
European
Moho
Iberian
Moho
Depth (km)
Latitude (deg)

Figure 3

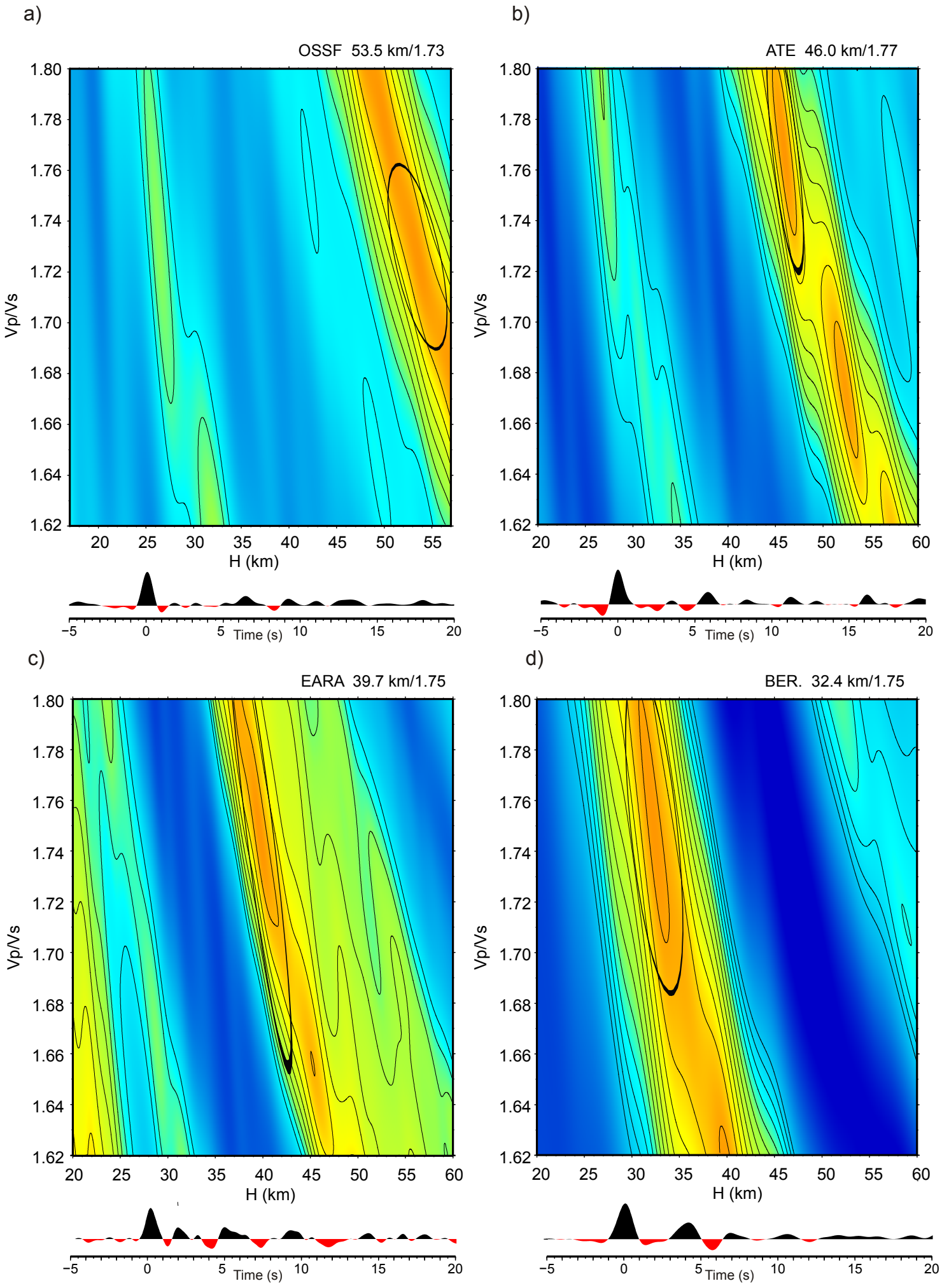
a)
OSSF 53.5 km/1.73
b)
ATE 46.0 km/1.77
c)
EARA 39.7 km/1.75
d)
BER. 32.4 km/1.75
Vp/Vs
H (km)
Time (s)

Figure 4

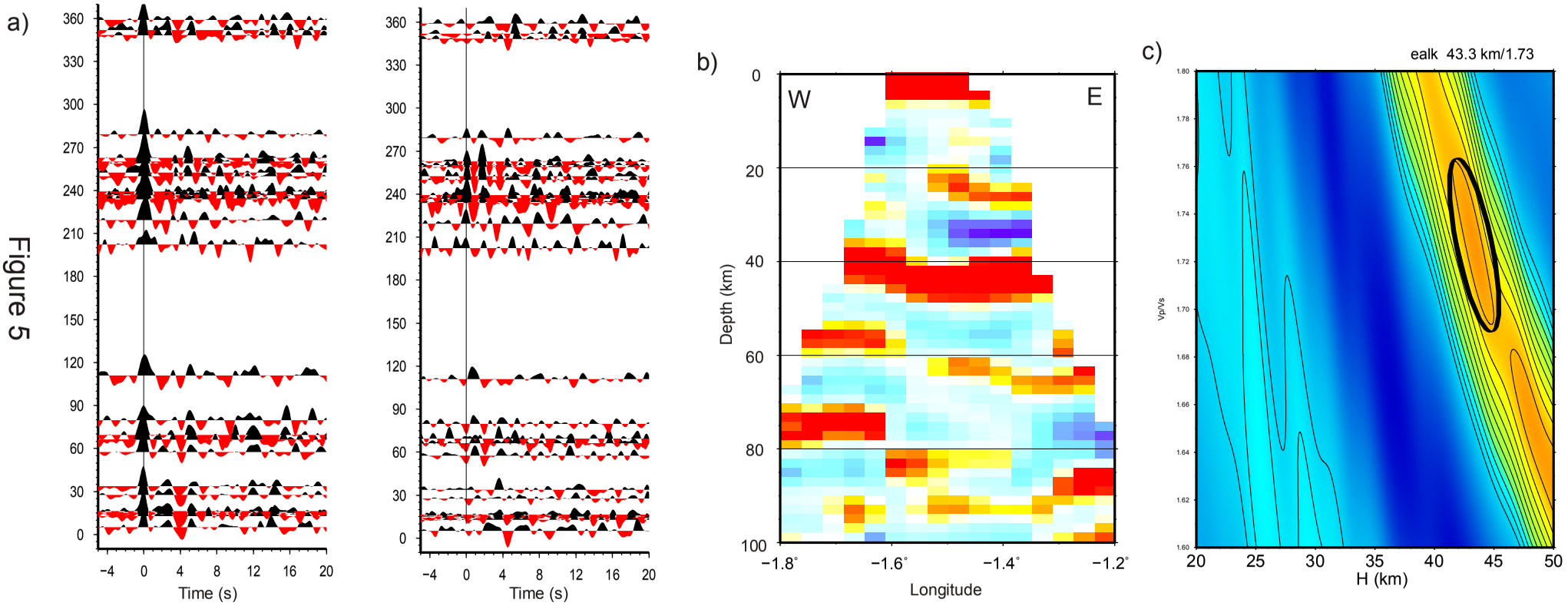
a)
360
330
300
270
240
210
180
150
120
90
60
30
0
−4
0
4
8
12
16
20
Time (s)
Time (s)
b)
W
E
Depth (km)
0
20
40
60
80
100
−1.8˚
−1.6˚
−1.4˚
−1.2˚
Longitude
c)
ealk 43.3 km/1.73
Vp/Vs
1.80
1.78
1.76
1.74
1.72
1.70
1.68
1.66
1.64
1.62
1.60
20
25
30
35
40
45
50
H (km)

Figure 5

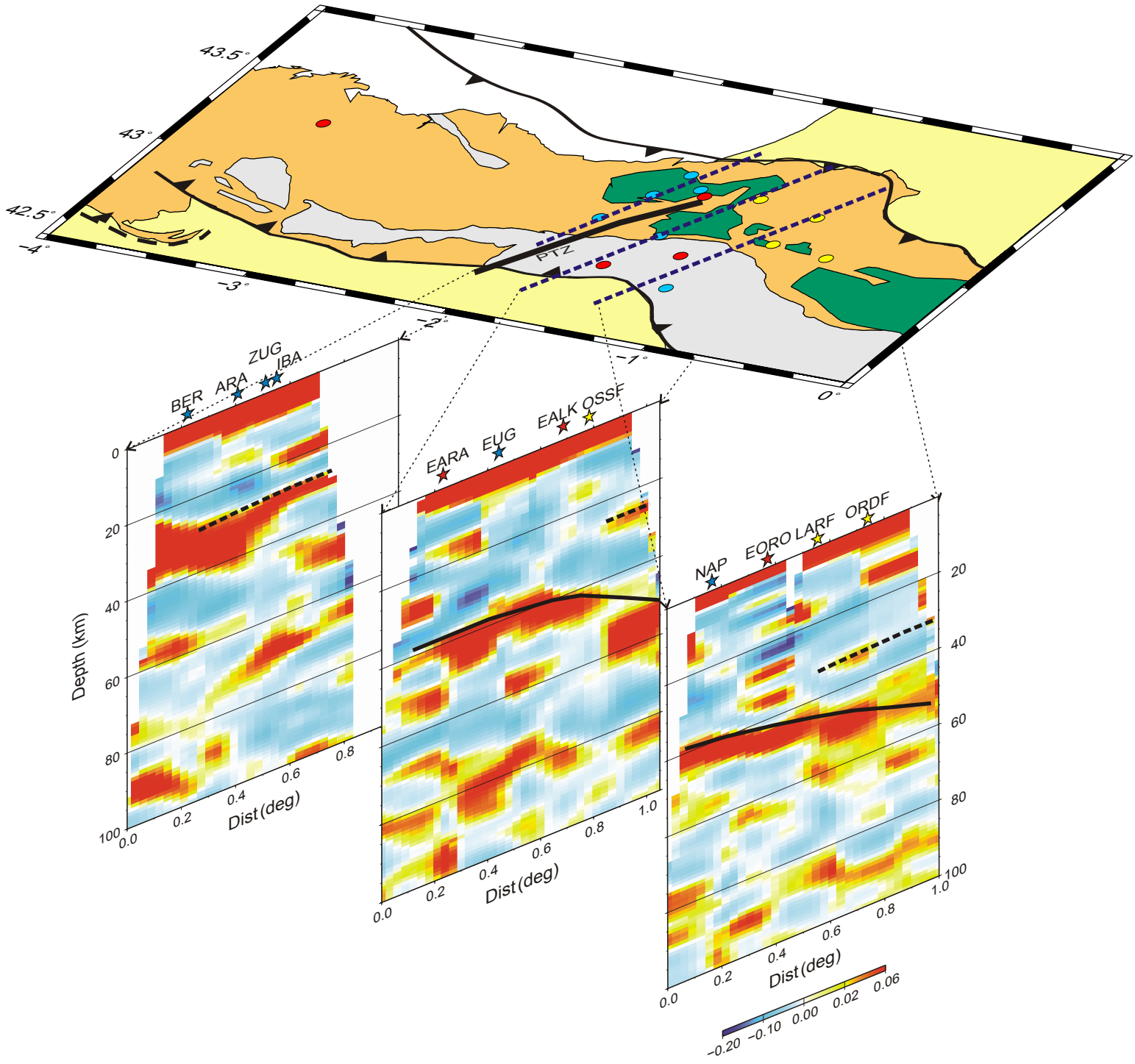
43.5°
43°
42.5°
-4°
-3°
-2°
-1°
0°
PTZ
BER
ARA
ZUG
IBA
EARA
EUG
EALK
OSSF
NAP
EORO
LARF
ORDF
Depth (km)
Dist (deg)
0.0
0.2
0.4
0.6
0.8
1.0
0
20
40
60
80
100
-0.20
-0.10
0.00
0.02
0.06

Figure 6

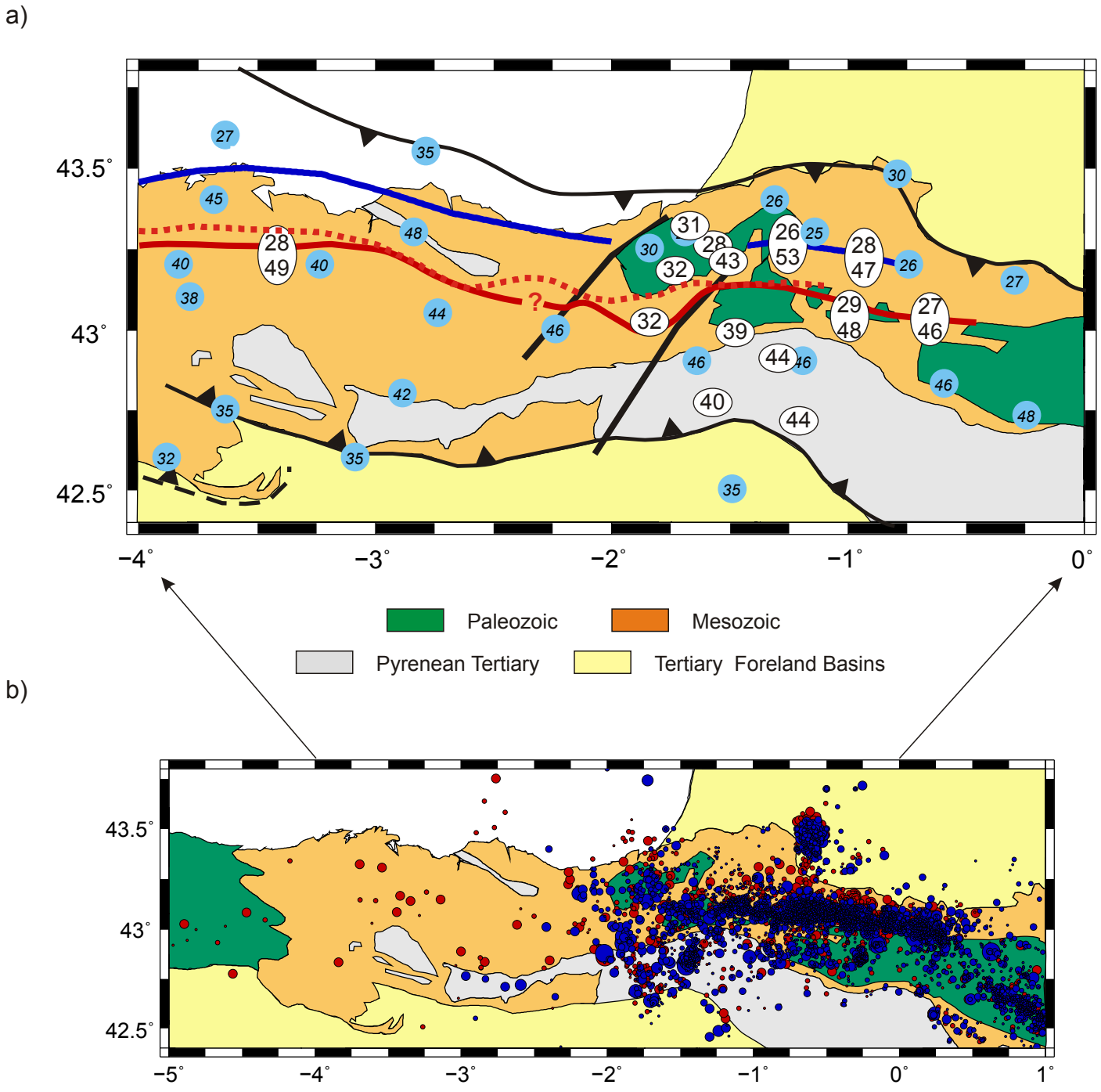
a)
43.5˚
43˚
42.5˚
−4˚
−3˚
−2˚
−1˚
0˚
Paleozoic
Mesozoic
Pyrenean Tertiary
Tertiary Foreland Basins
b)
43.5˚
43˚
42.5˚
−5˚
−4˚
−3˚
−2˚
−1˚
0˚
1˚

Figure 7